Electronic Supplementary Material (ESI) for Materials Chemistry Frontiers.
This journal is © the Partner Organisations 2018

Electronic Supplementary Information:

3D Confined Assembly of Polymer-Tethered Gold Nanoparticles into Size-Segregated Structures

Yi Yang,[#, a] Yulan Wang, [#, b] Seon-Mi Jin,[#, c] Jiangping Xu,[a] Zaiyan Hou,[a] Jingli Ren,[a] Ke Wang,[a] Eunji Lee,*[, c] Lianbin Zhang,[a] Yufeng Zhang,*[, b] and Jintao Zhu*[, a]

[a] Key Lab of Materials Chemistry for Energy Conversion and Storage of Ministry of Education (HUST), School of Chemistry and Chemical Engineering, Huazhong University of Science and Technology, Wuhan 430074, P. R. China

E-mail: jtzhu@mail.hust.edu.cn (J. Z.)

[b] State Key Lab Breeding Base of Basic Science of (Hubei-MOST) and Key Lab of oral Biomedicine, Ministry of Education, School and Hospital of Stomatology, Wuhan University, Wuhan 430079, P. R. China

E-mail: zyf@mail.whu.edu.cn (Y. Zhang)

[c] School of Materials Science and Engineering, Gwangju Institute of Science and Technology Gwangju 61005, R. Korea

E-mail: eunjilee@mail.gist.ac.kr (E. Lee)

[#] These authors contributed equally to this work.

Experimental Details

Synthesis of gold nanorods (GNRs): AuNRs were synthesized through the previously reported method.[1] The seed solution was prepared by mixing CTAB (5 mL 0.2 M), $HAuCl_4 \cdot 3H_2O$ (2.5 mL, 1 mM), $NaBH_4$ (0.6 mL, 10 mM) and 2.5 mL deionized H_2O in ice cold water. Growth solution contained CTAB (19 mL, 0.1 M), $HAuCl_4 \cdot 3H_2O$ (1 mL, 10 mM) and $AgNO_3$ (0.2 mL of 10 mM). After adding ascorbic acid (0.12 mL, 0.1 M), the dark-yellow solution turned colorless. Then, 0.32 mL seed solution was added to the growth solution. The formed GNRs were purified using centrifugation at 10,000-12,000 rpm.

Synthesis of spherical magnetic nanoparticles (MNPs): Fe_3O_4 MNPs were synthesized through the previously reported method.[2] The iron-oleate complex was prepared by reacting iron chlorides and sodium oleate. 36 g iron-oleate complex and 5.7 g oleic acid were dissolved in 200 g 1-octadecene at room temperature. The mixture was heated to 320 °C with a constant heating rate of 3.3 °C min-1, and then kept at that temperature for 30 min. After cooling down to the room temperature, 500 ml ethanol was added to precipitate the NPs. The MNPs were separated through centrifugation.

Synthesis of upconversion nanoparticles (UCNPs): $NaYF_4$:Yb/Er UCNPs were synthesized through the previously reported method.[3] ErCl3·6H2O (0.01 mmol), $YbCl_3 \cdot 6H_2O$ (0.1 mmol) and $YCl_3 \cdot 6H_2O$ (0.39 mmol) were added into a mixture of oleic acid (3 mL) and 1-octadecene (7.5 mL), and stirring at 150 °C for 0.5 h under a nitrogen atmosphere. After cooling down to room temperature, NH_4F (2 mmol) and NaOH (1.25 mmol) in 5 mL methanol solution were added and then heated to 70 °C for 0.5 h to remove the methanol. The temperature was kept at 120 °C for 10 min and then heated to 300 °C at a heating rate of 15 °C min^{-1}. After 1 h, the solution was cooled down to room temperature. The UCNPs were separated through centrifugation.

Transmission Electron Microscope (TEM): TEM investigation was performed on a JEOL 2100 LaB6 or FEG TEM operated at an acceleration voltage of 200 kV. TEM samples were prepared on 300 mesh copper grids covered with carbon film.

Scanning Electron Microscope (FEG-SEM): FEG-SEM (Nova Nano SEM 450) operated at voltage 10 kV. Samples for SEM were prepared by casting one drop of the assemblies on silicon wafers, and dried at room temperature.

Transmission Electron Microscopy Tomography (TEMT): TEMT measurements were performed on a JEM-1400 LaB6 (JEOL) operated at an acceleration voltage of 120 kV. TEMT samples were prepared on 300 mesh copper grids covered with carbon film. The tilt series of TEM images were recorded using a 1k×1k charge-coupled device (CCD) camera (JEOL) and a veleta 2k×2k CCD camera (Olympus). Pre-alignment of tilt series was done and fine alignment was executed using the IMOD software package. After the alignment, 3D images were reconstructed using the back projection algorithm. Subsequently, nonlinear anisotropic diffusion filter was used to reduce the noise of the reconstruction of the GNPs hybrid assemblies. 3D volumes (Figure 1 and Figure S5) were segmented using UCSF chimera. The small and large GNPs in the hybrid assemblies were labeled in red and yellow, respectively.

- Electron tomography acquisition conditions:

1) For Fig. 1d,1e: hybrid GNPs assembly of 15 nm@PS_{2K} and 8 nm@PS_{20K}

Angular sampling: - 70° to + 67° angles with 1° increment steps

Magnification: 80Kx

Pixel size: 0.32 nm for images

2) For Fig. 1i, 1j: hybrid GNPs assembly of 8 nm@PS_{2K} and 15 nm@PS_{20K}

Angular sampling: - 70° to + 66° angles with 1° increment steps

Magnification: 60K×

Pixel size: 0.43 nm for images

3) For Fig. S3: hybrid GNPs assembly of 8 nm@PS2K and 8 nm@PS20K

Angular sampling: - 60° to + 60° angles with 2° increment steps

Magnification: 60K×

Pixel size: 1.19 nm for images

UV-Vis Spectroscopy: Assemblies in aqueous solution were placed in quartz sample cell with a 0.7 cm cell path length. Absorption spectra (ranged from 400 nm to 1100 nm) were recorded by using LAMBDA 45 UV-Vis spectrophotometer (Perkin Elmer) at 25 °C with reference spectrum of deionized water.

Light to Heat Conversion: Assemblies aqueous solutions in Eppendorf tubes were irradiated upon laser at power density of 1.2 W/cm^{-2} for 5 min, and then the laser was turned off. The laser spot was adjusted to cover the whole surface of samples. Pure water was used as a negative control. Real-time thermal imaging of samples was recorded using a FLIR thermal camera and quantified by FLIR Examiner software.

Dynamic light scattering (DLS) characterization: The GNPs dispersion in distilled water were analyzed for assemblies size using dynamic light scattering (DLS, Zetasizer Nano ZS series, Malvern Instruments) with 532 nm laser wavelength.

X-ray photoelectron spectroscopy (XPS) measurements: 8 nm GNPs with different PS molecular

weight were dispersed on silicon wafers. XPS measurements were taken on a VG ESCALAB 250 spectrometer with an Al KαX-ray source (1486 eV), X-ray radiation (15 kV and 10 mA).

Contact angle measurement: The water contact angles were measured and captured on an optical contact-angle measuring device (JC2000C1, Dataphysics Instruments Shanghai Zhongchen Digital Technic Apparatus co., ltd).

Photothermal effect of GAs on killing bone-tumor cells in vitro: For photothermal effect test, cells were seeded into 96-well plate at the density of 5000 cells/well for 24 h. Then, the cells were treated with GAs at different concentrations. Subsequently, the cells were irradiated by 655 nm laser with a power density of 1.2 W cm^{-2} for 5 min. Cells treated with GAs in same condition without laser irradiation, cells in pure culture medium with or without laser irradiation were set as control. 12 h after the irradiation, cell viability was examined by CCK-8 assays. The culture medium was removed, and then 100 □L of CCK-8 mixture (reagent: culture medium = 1:10) was added into each well for 2 h. The mixture was the extracted in a new 96-well plate for reading at 450 nm on a plate reader (Biotek instruments, USA). Three replicates were carried out per sample.

1. W. Li, P. Zhang, M. Dai, J. He, T. Babu, Y.-L. Xu, R. Deng, R. Liang, M.-H. Lu, Z. Nie, J. Zhu, *Macromolecules* **2013**, *46*, 2241.

2. J. Park, K. An, Y. Hwang, J. Park, H. Noh, J. Kim, J. Park, N. Hwang, T. Hyeon, *Nat. Mater.* **2004**, *3*, 891.

3. B. Xu, X. Zhang, W. Huang, J. Yang, Y. Ma, Z. Gu, T. Zhai, Y. Zhao, *J. Mater. Chem. B* **2016**, *4*, 2776.

Supplementary Table:

Table S1. The XPS characterization of the GNPs. Hydrophilicity of the GNPs can be judged by the intensity of the hydrophilic group signal (CTAB). The proportion of N element decreased with the increasing of modified PS length, suggesting that hydrophilicity is overlaid gradually.

	Atomic Concentration (%)					
	C	**O**	**Au**	**S**	**N**	**Br**
8 nm@PS_{2K}	88.25	6.21	1.32	0.94	3.16	0.12
8 nm@PS_{5K}	90.27	5.53	0.48	0.65	2.95	0.12
8 nm@PS_{12K}	90.69	7.11	0.22	0.35	1.49	0.14
8 nm@PS_{20K}	92.37	6.11	0.14	0.36	0.94	0.12

Supplementary Figures:

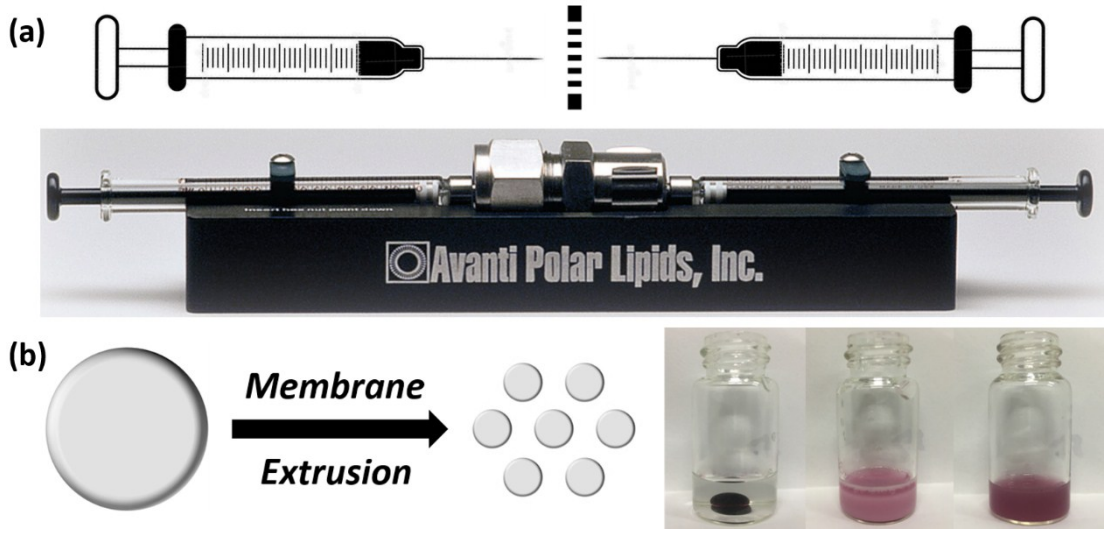

Figure S1. (a) Illustration showing the membrane extrusion device for preparing emulsion droplets. (b) Illustration showing the membrane extrusion process, and photographs for the process of emulsion solvent evaporation approach. Through membrane extrusion, organic phase was turned into droplets (~ 1.2 μm). Gold assemblies were obtained via removal of the organic solvent.

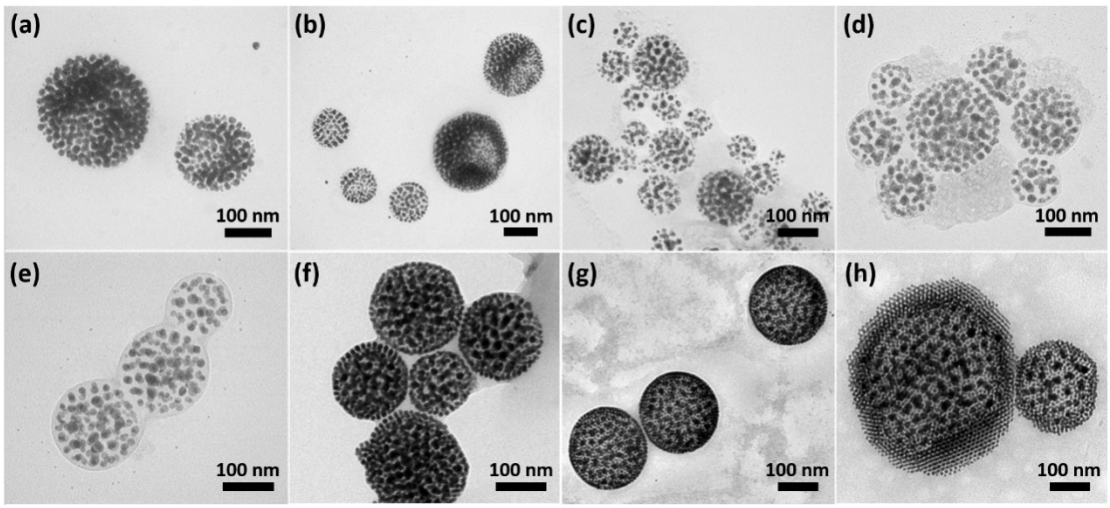

Figure S2. TEM images of the assemblies: (a) 8 nm@PS_{2K}+15 nm@PS_{2K}, (b) 8 nm@PS_{2K}+ 15 nm@PS_{5K}, (c) 8 nm@PS_{5K} +15 nm@PS_{12K}, (d) 8 nm@PS_{12K}+15 nm@PS_{20K}, (e) 8 nm@PS_{20K}+ 15 nm@PS_{20K}, (f) 8 nm@PS_{2K}+15 nm@PS_{12K}, (g) 8 nm@PS_{5K}+15 nm@PS_{20K}, (h) 8 nm@PS_{2K} + 15 nm@PS_{20K}. When the difference between the molecular weight of modified polymer decreased, core-shell segregation behavior of the GNPs would become weaker.

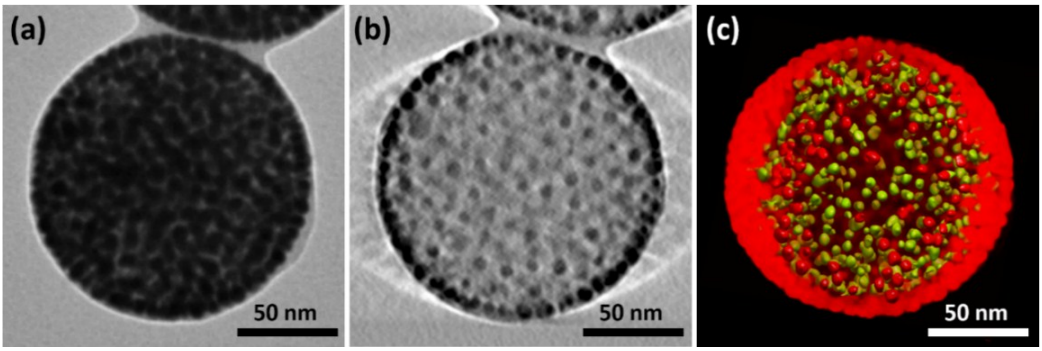

Figure S3. (a) TEM image of the assemblies combined from 8 nm@PS_{2K} and 8 nm@PS_{20K}, (b, c) the related TEMT result. (b) Slice image of 3D tomographic reconstruction of (a). (c) 3D volume image resulted from TEMT. Clearly, GNPs on the surface arranged more closely than that in the interior, indicating that phase separation takes place and the short chain group still distributes the location outward.

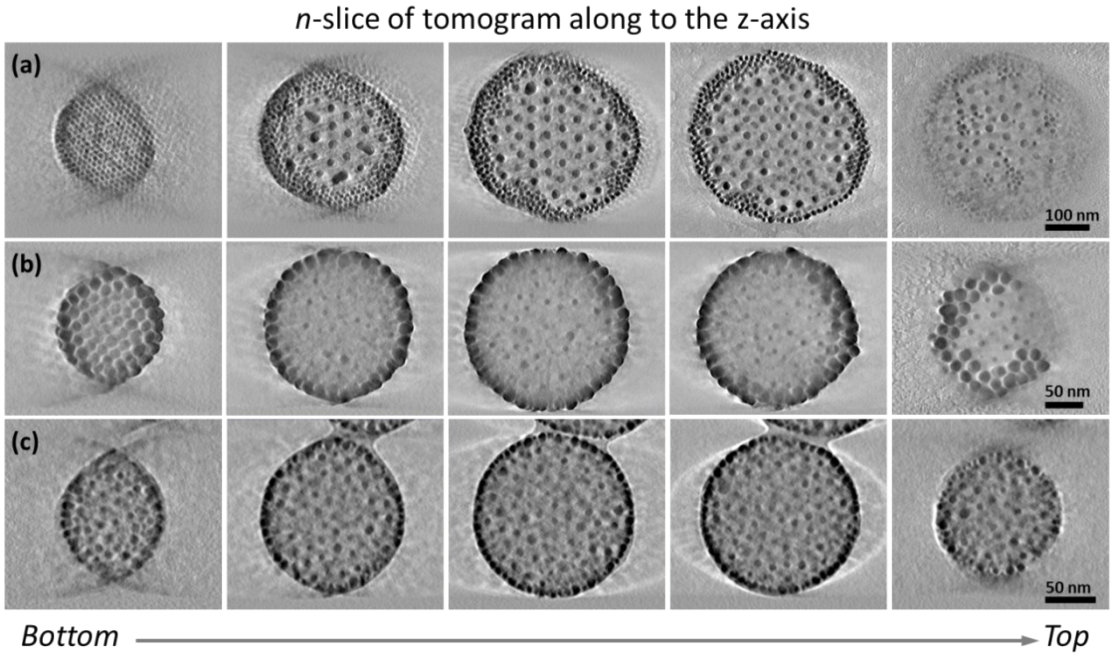

Figure S4. Images of selected computational xy-slices of the 3D tomographic volume of a tilt series of hybrid GNPs assemblies composed of (a) 15 nm@PS_{20k} and 8 nm@PS_{2k}, (b) 15 nm@PS_{2k} and 8 nm@PS_{20k}, and (c) 8 nm@PS20k and 8 nm@PS2k, clearly revealing the size-segregated core-shell structure. The intervals in z-direction between consecutive slices are (a) 14.9 nm, (b) 17.5 nm and (c) 35.7 nm, respectively. The voxel sizes in z-axis are 0.43 nm for (a), 0.32 nm for (b), and 1.19 nm for (c).

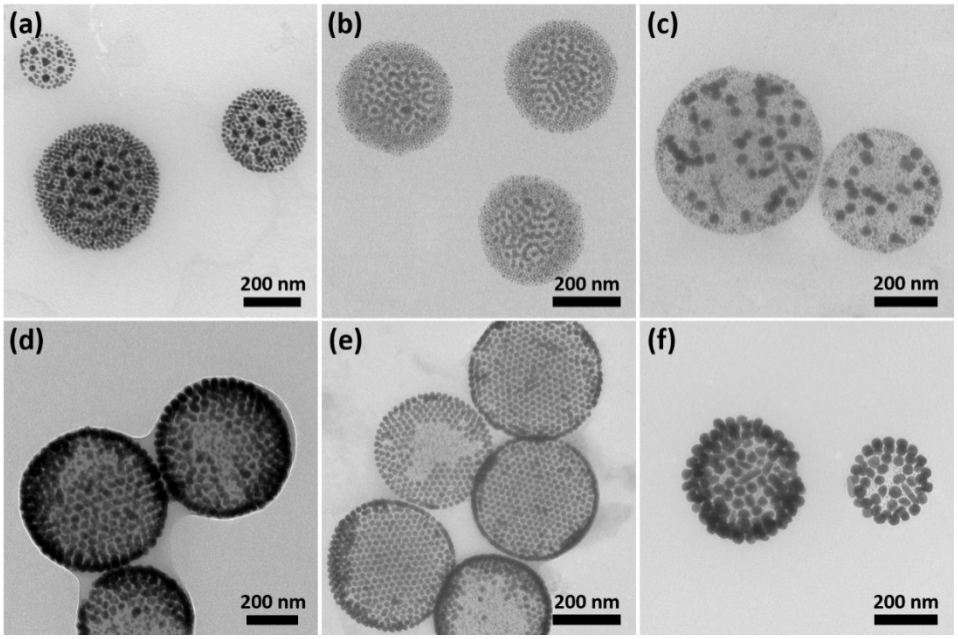

Figure S5. GNPs combination of different sizes was studied: (a, d) TEM image of the combination of 8 and 24 nm, with the size ratio of about 1:3; (b, e) combination of 3.5 and 15 nm, with the size ratio of about 1:5; (c, f) combination of 3.5 and 30 nm, with the size ratio of about 1:10. The inner/outer distribution of the large/small GNPs can still be effectively regulated by varying the Mw of the modified PS.

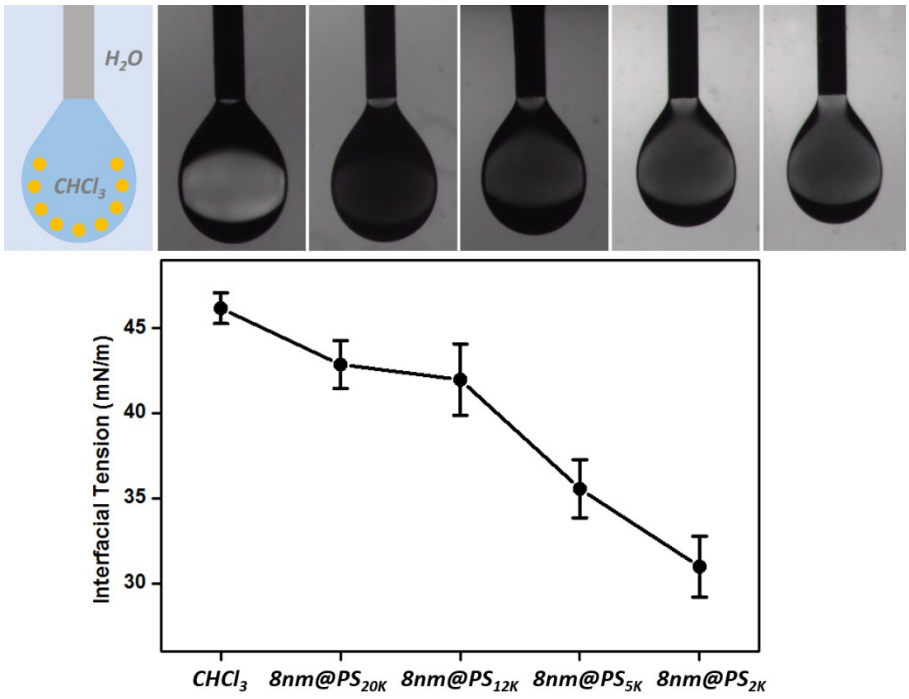

Figure S6. The hydrophilicity of the GNPs was determined by the contact angle of the oil/water interface. Top optical microscopy images are the pendent drops for the measurement of interfacial tension, while down plot shows the interfacial tension as a function of PS M_w. Because GNPs will diffuse to the boundary, the presence of hydrophilic GNPs in chloroform will reduce the interfacial tension. With the decrease of modified PS M_w, the interfacial tension declined gradually, indicating that GNPs exhibit stronger hydrophilicity. Concentration of different GNPs were all kept at 8×10^{-9} mol/mL. Error bars represent the standard deviation.

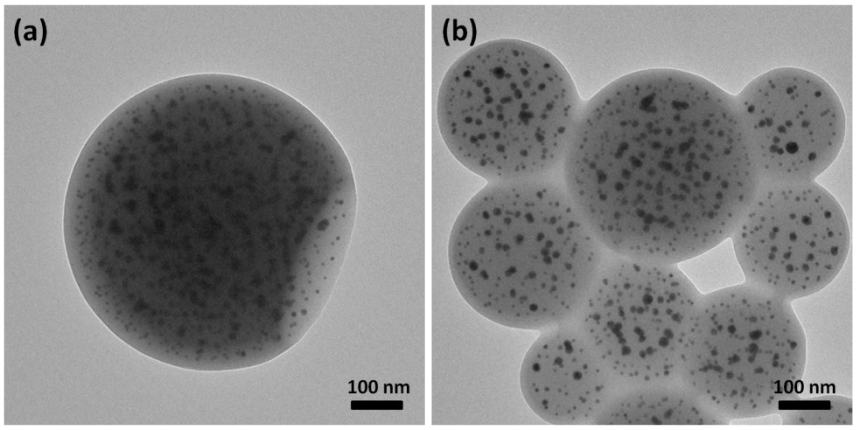

Figure S7. TEM images of the assemblies when 8 nm@PS_{20K} and 15 nm@PS_{50K} are employed. Clearly, no obvious segregation occurs in the assemblies even if their molecular weight difference reached 30K.

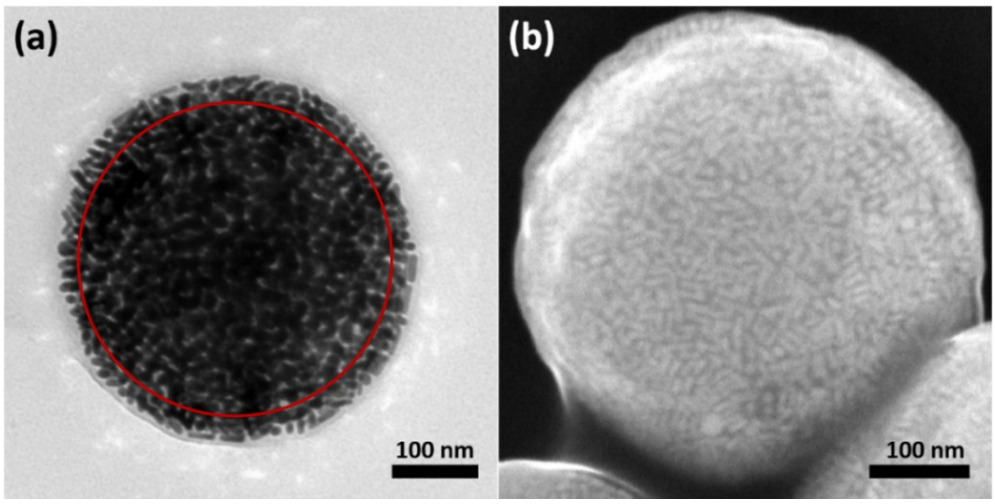

Figure S8. (a) and (b) are the TEM and SEM images of assemblies combined with GNPs and GNRs. GNRs are modified with PS_{2K} while GNPs are modified with PS_{12K}. The shape and diameter are the basis for distinguishing GNRs and GNPs. Clearly, GNRs distribute on the surface of the assemblies.

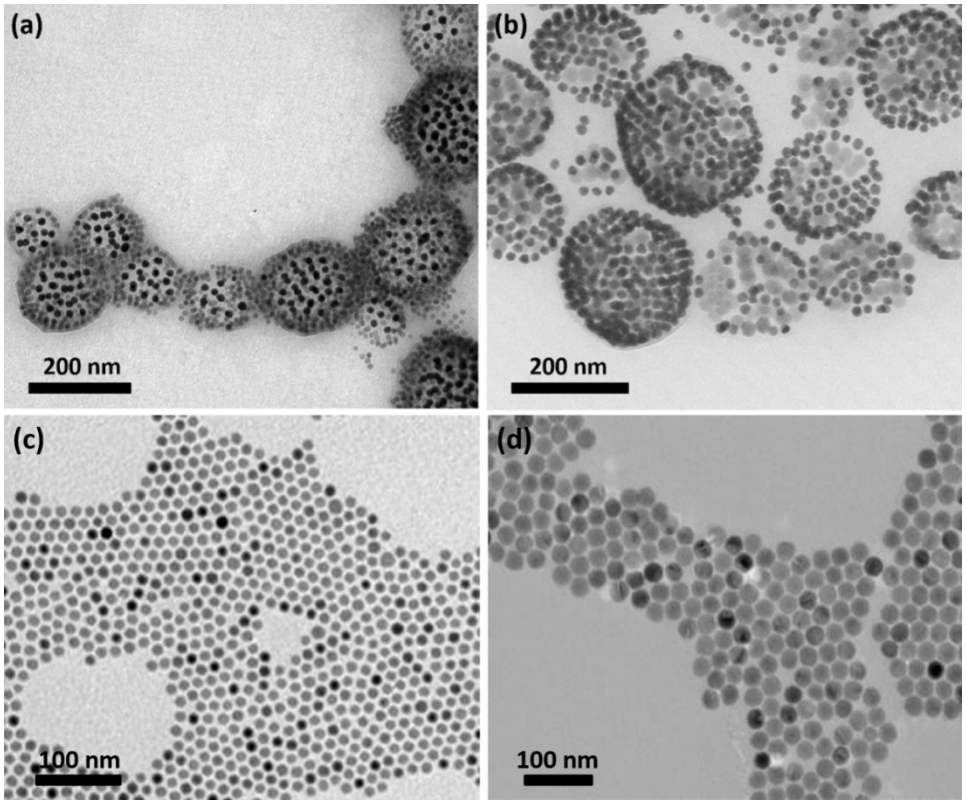

Figure S9. (a, b) Different kinds of polymer-tethered nanoparticles were combined for co-assembly: (a) PS_{2K}-tethered MNPs and PS_{20K}-tethered GNPs co-assemble to core-shell structure, where GNPs form the core while MNPs form the shell. (b) PS_{2K}-tethered GNPs and PS_{20K}-tethered UCNPs co-assemble to core-shell structure, where UCNPs form the core while GNPs form the shell. (c, d) TEM images for the individual monodisperse MNPs (a) and monodisperse UCNPs (d) after PS modification.

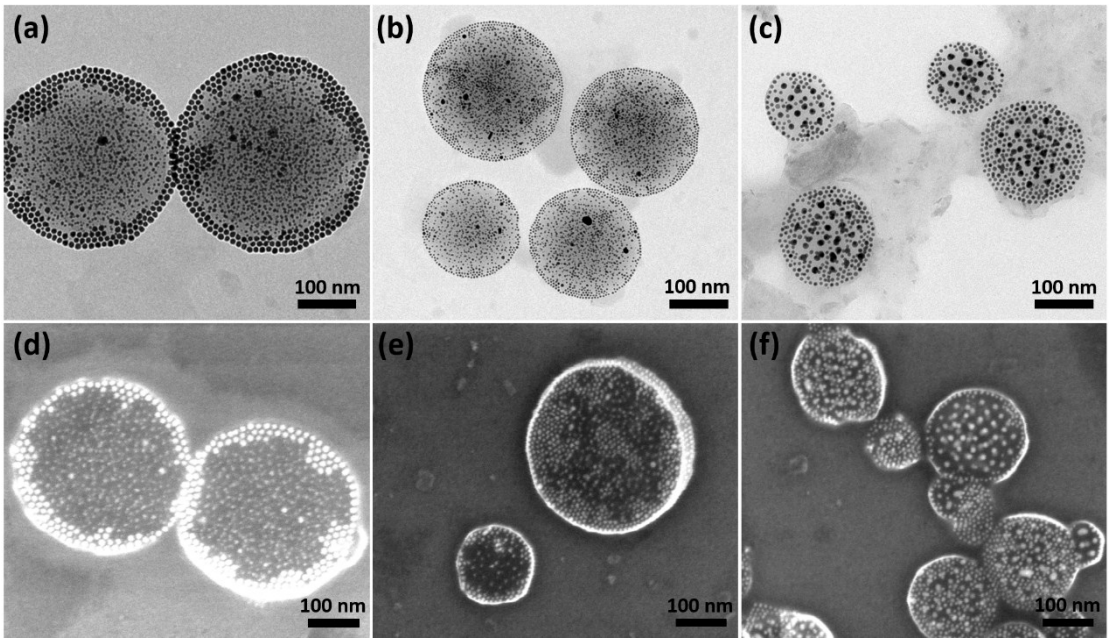

Figure S10. TEM images of the assemblies after fast solvent evaporation within 1h: (a) 15 nm@PS_{2K}+8 nm@PS_{20K}, (b) 8 nm@PS_{2K}+8 nm@PS_{20K} and (c) 8 nm@PS_{2K}+15 nm@PS_{20K} and corresponding SEM images (d-f). Collapsed assemblies (or disk-like structures) with central LGNPs and SGNPs were observed for these samples. Presumably, fast solvent evaporation will quickly lead to the migration of SGNPs to the oil/water interface, and form gel-like shell of the emulsions due to the high local concentration of the SGNPs at the oil/water interface. In this case, the gel-like shell of the emulsion will not shrink fully to form the core-shell assemblies, but form hollow assemblies with SGNPs at the surface and LGNPs at the inner layers of the capsules. The hollow assemblies will collapse and generate disc-like structures during sample preparation and electron microscopy investigation.

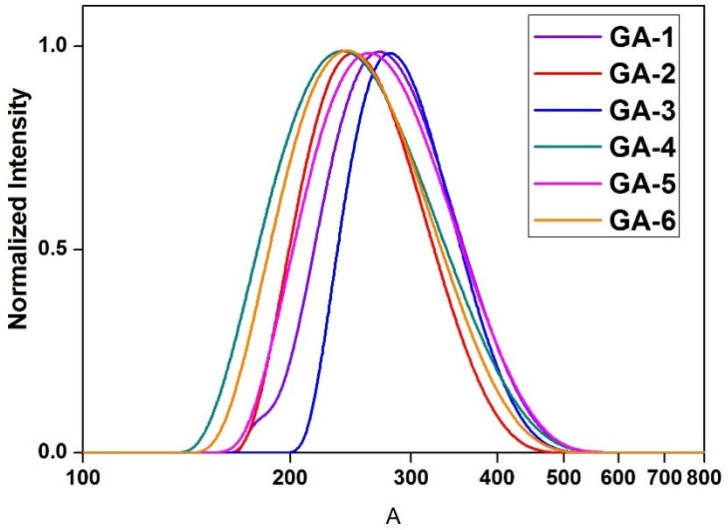

Figure S11. The size of GNPs assemblies from GA-1 to GA-6 was characterized by DLS. Size of the GAs for the 6 groups ranged from 220 nm to 300 nm.

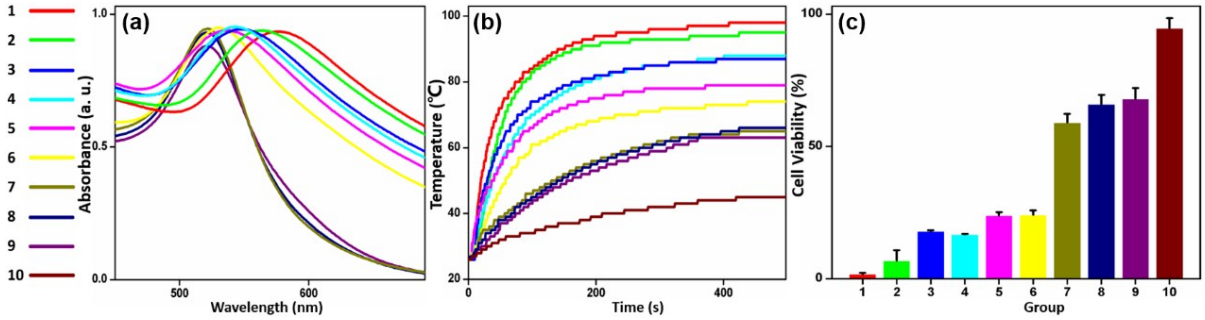

Figure S12. (a-c) UV-Vis absorption spectra, photothermal effect and killing effect on the MG-63 cells from groups 1-10 at 200 μg/mL under 655 nm laser. Groups include (1) assemblies of single GNPs-15 nm@PS_{2K}, (2) assemblies of single GNPs-8 nm@PS_{2K}, (3) hybrid assemblies of GNPs-15 nm@PS_{2K} and GNPs-8 nm@PS_{20K} (1:1), (4) hybrid assemblies of GNPs-15 nm@PS_{20K} and GNPs-8 nm@PS_{2K} (1:1), (5) assemblies of single GNPs-15 nm@PS_{20K}, (6) assemblies of single GNPs-8 nm@PS_{20K}, (7) GNPs-15 nm, (8) mix of GNPs-8 nm and GNPs-15 nm (1:1) and (9) GNPs-8 nm. In (b), (10) is the pure water without GNPs. In (c), (10) is the group without GNPs with laser irradiation.

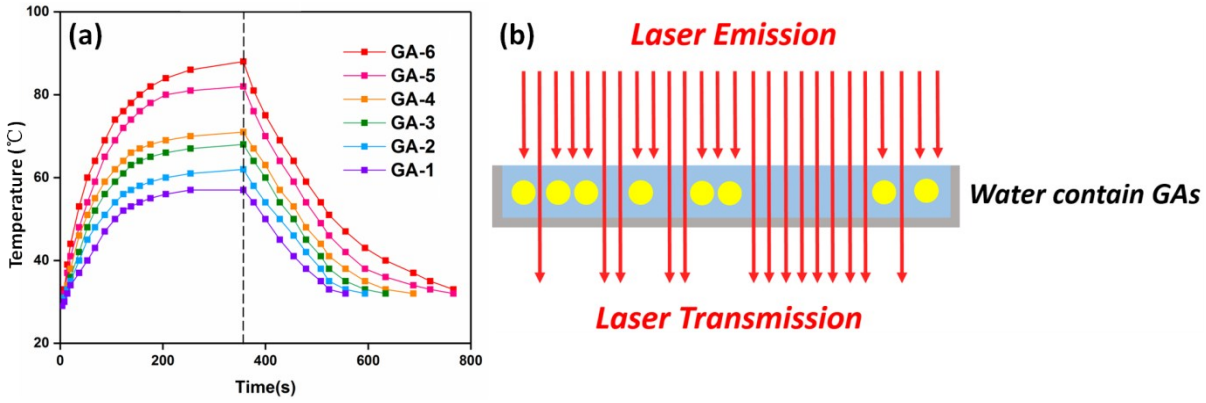

Figure S13. (a) Heat/cool experiment of GAs aqueous solution under 1.2 W cm^{-2} 655 nm irradiation. The photothermal conversion efficiencies can be estimated by the following formula: $\eta=(hS\Delta T-Q_s)$ / $I(1-10^{-A655})$ and $\tau_s=mC$ / hS. For example, τ_s of GA-6 is calculated to be 165.38 according to the cooling rate of sample. hS is equal to 0.00254, $A655$ is measured by Lambert Beer's law. η of GA-1 to GA-6 is calculated to be 7.1%, 8.36%, 9.9%, 10.6%, 13.7%, 15.2%, respectively. (b) Illustration showing the photothermal conversion experiments. Under 655 nm laser irradiation, GAs in water can absorb part of the laser energy and convert to the heat due to the small amount of the GAs. However, most laser beams pass through the orifice plates and water, which are not absorbed by the GAs. Presumably, this is the main reason why the calculated photothermal conversion efficiency is very low.

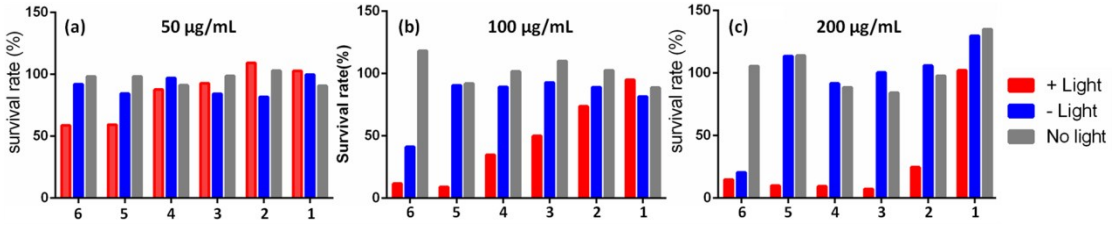

Figure S14. (a-c) plots demonstrate the ability of killing MG-63 cells under different concentrations, +light denotes groups with GAs and laser irradiation, -light denotes groups with laser irradiation only, No light denotes groups with GAs without laser irradiation.